

Single scan STEM-EMCD in 3-beam orientation using a quadruple aperture

Hasan Ali^{a,b,1,*}, Sharath Kumar Manjeshwar Sathyanath^b, Cheuk-Wai Tai^a, Jan Ruzs^c,
Toni Uusimäki^a, Björgvin Hjörvarsson^c, Thomas Thersleff^a, Klaus Leifer^b

^a Department of Materials and Environmental Chemistry, Stockholm University, 106 91 Stockholm, Sweden

^b Department of Materials Science and Engineering, Uppsala University, Box 534, 75121, Uppsala, Sweden

^c Department of Physics and Astronomy, Uppsala University, Box 516, 751 20 Uppsala, Sweden

ABSTRACT

The need to acquire multiple angle-resolved electron energy loss spectra (EELS) is one of the several critical challenges associated with electron magnetic circular dichroism (EMCD) experiments. If the experiments are performed by scanning a nanometer to atomic-sized electron probe on a specific region of a sample, the precision of the local magnetic information extracted from such data highly depends on the accuracy of the spatial registration between multiple scans. For an EMCD experiment in a 3-beam orientation, this means that the same specimen area must be scanned four times while keeping all the experimental conditions same. This is a non-trivial task as there is a high chance of morphological and chemical modification as well as non-systematic local orientation variations of the crystal between the different scans due to beam damage, contamination and spatial drift. In this work, we employ a custom-made quadruple aperture to acquire the four EELS spectra needed for the EMCD analysis in a single electron beam scan, thus removing the above-mentioned complexities. We demonstrate a quantitative EMCD result for a beam convergence angle corresponding to sub-nm probe size and compare the EMCD results for different detector geometries.

1. Introduction

The discovery and subsequent experimental realization of electron magnetic circular dichroism (EMCD) measurements [1] in the transmission electron microscope (TEM) opened the door to characterize the local structure and magnetic properties of magnetic materials at nanometer to atomic scale. The experimental development over the last more than 15 years [2] made it possible to characterize the magnetic moments of single atomic planes [3,4] and atomic site-specific magnetic measurements [5]. The technique has been used to detect the magnetic ordering in an antiferromagnet [6] and has been used to correlate the magnetic properties to structural changes at nano scale [7–11]. Despite the remarkable progress in optimizing and improving the experimental conditions [12–17], there are still critical challenges associated with the EMCD experiments which enhance the level of difficulty in carrying out and interpreting the results of such experiments. The major challenges include poor signal to noise ratio of the EMCD signal, its strong dependence on dynamical diffraction effects, high sensitivity to crystal orientation conditions and multiple acquisitions needed in an EMCD experiment.

In the initial experimental setup proposed by Schattschneider et al. [1], TEM specimen is tilted to a 2-beam condition (2BC) and

subsequently two electron energy loss spectra (EELS) are acquired at conjugate scattering angles. The EMCD signal is obtained by taking the difference of these two EELS spectra after standard post-processing. This is perhaps the simplest and experimentally most convenient diffraction condition as it can yield maximum EMCD signal strength and needs only two acquisitions. However, there are certain critical challenges associated with this condition which arise due to the asymmetry of the 2BC [18,19]. This asymmetry leads to strong dependence of the EMCD signal strength on slight changes in the diffraction conditions. In our previous work using a customized aperture, we showed that a misalignment as small as 2 mrad from the perfect 2BC is sufficient to significantly diminish the EMCD signal [20]. Due to slight imperfections in crystal structures, there are high chances to encounter such tiny mistilts specially in a STEM map. In addition to weakening the strength of the EMCD signal, these small orientation changes may also lead to difficulties in post-edge normalization (discussed below), making the quantitative analysis cumbersome. So perhaps this diffraction geometry is suitable mainly for the detection of EMCD signal or the qualitative analysis but poses critical challenges for a quantitative analysis.

EMCD experiments can also be carried out under zone axis conditions which ensures that the atomic columns are parallel to the electron beam, opening the prospects for atomically resolved EMCD

* Corresponding author.

E-mail address: ali.hasan@angstrom.uu.se (H. Ali).

¹ Present address: Ernst Ruska-Centre for Microscopy and Spectroscopy with Electrons and Peter Grünberg Institute, Forschungszentrum Jülich, 52425 Jülich, Germany.

measurements, which are not possible under 2 or 3-beam conditions. However, executing EMCD experiments under a zone axis is very challenging due to the complex distribution of the magnetic signal around the Bragg spots [21,22]. In addition, the relative strength of the magnetic signal is much lower compared to 2 or 3-beam conditions. In our previous work, we used complex shaped hardware apertures to detect the zone axis EMCD signals [23,24]. The EMCD signal in a zone axis is also strongly influenced by small orientation changes, shown theoretically [19] and experimentally [23]. Due to the severe challenges associated with zone axis EMCD, this approach is the most challenging from an experimental point of view, ideally reserved for scientific questions where atomic resolution is truly required.

Another possible diffraction geometry for the EMCD experiments is a 3-beam condition (3BC) where two diffracted spots $\pm \mathbf{G}$ are equally excited around the direct beam. The EMCD signal has four magnetic components in this case marked by white circles in Fig. 1 (c). Here ++ and -- represent the EELS spectra carrying positive chirality whereas +- and -+ represent the EELS spectra with negative chirality. In a conventional 2BC, the EMCD signal is obtained by taking a single difference between either ++ and +- or between -+ and -- whereas in this case, the two differences are added together to obtain a double difference. It has been shown that the double difference approach is more robust against the small misalignments of the crystal [18] and largely mitigates the asymmetric effects encountered in single difference case [19]. Although the magnetic signal strength is comparatively weaker in the 3BC than the 2BC [12], it is nevertheless sufficient for quantitative EMCD analysis. Here, the robustness against the asymmetric effects makes it the most favorable overall choice for quantitative EMCD experiments.

Another important factor to consider is the obtainable spatial resolution of analysis which makes EMCD superior to complementary techniques such as XMCD [25]. The initial experimental setup proposed by Schattschneider et al. [1] uses a parallel electron beam to illuminate the sample. The spatial resolution of EMCD analysis is defined by the diameter of the electron beam which, in the case of parallel illumination, is limited to few tens of nanometers or at the best can reach to a couple of nanometers by converging the beam [26]. The alternative route to achieve higher spatial resolution is to carry out the EMCD experiments in scanning TEM (STEM) mode. In STEM-EMCD experiments [27], a finely focused electron probe is scanned across a well-defined area of the specimen and an EELS spectrum is acquired at each probe position, for multiple off-axis detector positions. With the recent advances in probe-correctors, it is possible to focus the probe to be smaller than low order atomic plane distances, permitting atomic-plane EMCD measurements to be performed when the sample is tilted to 2BC or 3BC [4,28]. In addition to improving the spatial resolution, STEM-EMCD allows for

advanced statistical methods to be employed by acquiring hundreds of EELS spectra compared to single measurements done in the TEM mode, a greatly improved signal to noise ratio by integrating multiple spectra and an efficient dose distribution on the analyzed area of the sample [7, 29].

One highly problematic part in such an experiment is that the same area of the specimen must be scanned multiple times to acquire multiple STEM-EELS datasets at different off-axis aperture positions. The exact number of scans depends on the diffraction condition chosen for the experiment. To correlate the spectra in the multiple STEM-EELS datasets on a pixel-by-pixel basis, all the experimental conditions must remain the same during their acquisition, which is a non-trivial task. A slight specimen drift in between the multiple sequential scans can degrade the spatial registration and/or the orientation conditions under the electron probe. Also, the morphology of the specimen can change between multiple scans e.g. due to damage or contamination caused by high intensity electron probe. An ideal situation to remove all these complexities would be to acquire all the EELS spectra needed in an EMCD experiment in a single beam scan. While we have previously demonstrated such single pass STEM-EMCD experiments for the 2BC [30,20] and zone-axis conditions [24,23], the quantitative EMCD experiments under these conditions are challenging due to reasons discussed above.

Considering the advantages of double difference procedure, we here extend our experience to model single pass STEM-EMCD experiments for 3-beam diffraction geometry. We report an experimental setup using a quadruple aperture to simultaneously acquire four angle-resolved STEM-EELS datasets in a single scan. The application of double difference procedure on these four datasets yields a quantitative EMCD signal. We show that the double difference procedure to obtain the EMCD signal is more tolerant to small orientation changes and reduces complexities in the post-processing of the EELS spectra.

2. Experimental details

We used a 35 nm bcc Fe thin film grown on MgO (001) substrate for the investigations. The sample was fabricated as described in [24]. The TEM specimen was prepared in a plan view geometry by mechanical polishing, dimple grinding and subsequent Ar-ion milling to reach perforation. The quadruple aperture was made of Titanium. A three axis computer numerical control (CNC) machine was used for milling and drilling the holes using precision drills made of Tungsten. After the milling process, a lathe machine was used to cut the 3 mm aperture disc, followed by smoothing the surface. Deburring was followed to clean the holes to remove any material left from the above steps. Finally the aperture was subjected to ultrasonic bath for final cleaning.

The EMCD experiments were performed on a JEOL 2100F equipped

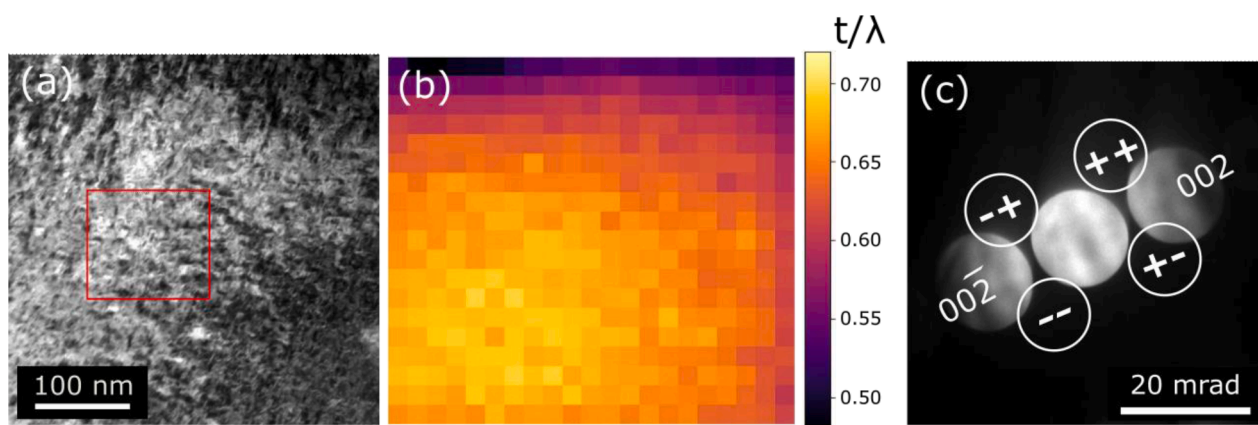


Fig. 1. Experimental Conditions for the single scan STEM-EMCD experiment. (a) survey image showing the area scanned during the experiment in a red box (b) thickness in terms of t/λ for the sample area used in the experiment (c) diffraction conditions showing the 3-beam orientation with $g = \pm 002$ excited. The aperture positions for the EMCD experiment are shown by white circles. The quadruple aperture was oriented such that the four aperture holes overlay these positions.

with a post column Gatan Tridiem imaging filter (GIF). The microscope was operated at an acceleration voltage of 200 kV. The quadruple aperture was installed at the spectrometer entrance plane in such an orientation that the four aperture holes do not overlap along q_y -axis in the diffraction plane. The microscope was switched to STEM mode and the convergence semi-angle was set to 7.5 mrad by changing the current in mini-condenser lens. The TEM specimen was tilted to a 3-beam condition from the [001] zone axis and manually rotated in the holder to orient the Bragg discs with respect to the four aperture holes according to the EMCD experimental requirements as shown in Fig. 1(c). Please note that the post-specimen lenses in most of the modern instruments can be used to rotate the diffraction pattern which would be easier than physically rotating the sample. In our case, we were already at the limit of tuning the post-specimen lenses for reducing the camera length to meet the experimental requirements (described in discussion section), so we had to additionally physically rotate the sample. A $120 \times 120 \text{ nm}^2$ well-oriented region of the specimen was chosen and the electron probe was scanned across this region. An in-house developed script was used to acquire the GIF CCD image at each probe position while keeping the GIF in EELS mode. This acquisition results in a 4DSTEM dataset where the first two dimensions represent the spatial coordinates of the specimen area whereas the later two dimensions are the energy loss and the momentum transfer along q_y as shown in Fig. 3. More information about such data acquisition mode can be found at [20,24,31,30]. The same area of the specimen was scanned once more to acquire the low-loss EELS spectra which were used for thickness determination. The low-loss EELS data was acquired on-axis by inserting standard circular aperture of the spectrometer.

3. Results

3.1. Simulations of EMCD signal under 3-beam condition

EMCD simulations were performed using MATS.v2 algorithm [32] for a 35 nm thick bcc Fe sample oriented in an exact three-beam orientation with Bragg spots $G = \pm 002$. The incoming beam was approximated by a plane wave at acceleration voltage of 200 kV. Figure 2 shows the result of simulations. The maximum EMCD signal predicted by the simulations for a thickness of 35 nm of Fe is somewhat between 4-5%. The strongest EMCD signal is concentrated in a limited q_x range while the selection of q_y is quite flexible. Therefore, q_x plays more decisive role to choose the four detectors' positions. It is evident that detector positions centered at conventional Thales position (marked by ++, +-, -+, -) are optimum for EMCD acquisition. Therefore, the quadruple aperture was designed in a way that the four aperture positions were symmetric and equidistance with respect to each other, making sure that all the apertures are located at similar angular positions (Thales circle positions) with respect to the Bragg spots.

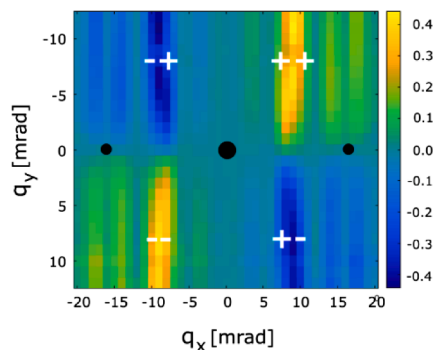


Fig. 2. Distribution of EMCD signal at L_3 energy loss edge of Fe with 35 nm thickness under 3-beam condition. The black dots represent the positions of direct beam and Bragg spots ($G = \pm 002$).

3.2. Experimental results

Figure 3 shows the CCD image of the quadruple aperture overlaid on the diffraction pattern (similar to Fig. 1(c)). The four aperture holes are named as A1, A2, A3 and A4. Switching to EELS mode and acquiring the CCD image under these conditions produces a 2D EELS image where the q_x axis is replaced by the energy dispersive axis and each value along q_y axis corresponds to the sum of intensities at scattering vectors $q_x \times q_y$ with q_x ranging between the left and right border of the aperture. The non-overlapping geometry of the apertures along q_y results in distinct momentum-resolved spectral domains (marked by ++, +-, -+, -) in the 2D EELS image as shown in Fig. 2. There is a slight overlap between these domains as the aperture holes were slightly overlapping along q_y . The four EELS spectra needed for the EMCD analysis are extracted from the 2D EELS image by integrating the intensity of each domain along the energy loss axis, avoiding the overlapping regions. The four extracted spectra are also shown in Fig. 3.

The relative thickness of the sample was determined by applying log-ratio method [33] to the low-loss EELS dataset acquired from the same region where EMCD experiment was performed. This method gives the thickness in terms of t/λ where t is the thickness of the specimen and λ is the mean free path of electrons transmitting through the specimen. The relative thickness map is shown in Fig. 1(b). It is worth noting that a 35 nm thickness of Fe is not ideal for the EMCD experiments [34] but should still result in a 4 % EMCD signal at L_3 energy loss edge of Fe as shown in Fig. 2. Moreover, the total thickness of the specimen in this experiment is also contributed by the MgO substrate below Fe film. To remove the plural scattering effects from this additional layer, we deconvolved the core-loss EELS spectra with the corresponding low-loss spectra by using Fourier-ratio deconvolution technique [35]. An interesting feature in the thickness map is the increasing thickness gradient from top to bottom although from our observations during the experiment, the thickness of the mapped area should be more or less homogeneous. As the low-loss EELS spectra were acquired after the EMCD map, a part of this thickness gradient is likely the result of contamination built on the sample during the first scan. This highlights one of the advantages of a single-pass EMCD experiment as the multiple scans needed for conventional STEM-EMCD will see a systematic contamination build-up following each individual scan, complicating the subsequent analysis (particularly regarding the removal of plural scattering) and diluting the already weak EMCD signal.

Figure 4 shows the four raw EELS spectra extracted from the 2D EELS image shown in Fig. 3. The corresponding deconvolved spectra are also shown in the same figure. It can be seen that the intensity of the post-edge after $\text{Fe-L}_{2,3}$ edges goes significantly down in the deconvolved spectra indicating the efficient removal of plural scattering effects. Another observation is that the number of electron counts in second and third spectra is higher than the first and fourth spectra. This is a consequence of slightly misaligned diffraction pattern with respect to the aperture holes which results in higher intensities within the diffracted discs' contributing more to aperture A2 and A3 than the other two apertures as can be seen in Fig. 3. Nevertheless, this difference is arising mostly from the non-magnetic signal and should be removed by normalizing the post-edge intensity of the spectra after background subtraction. As mentioned above, we expect the double difference procedure to largely eliminate such effects caused by asymmetry of the diffraction geometry as well as detectors' position.

To test whether the double difference procedure really helps to compensate the asymmetry and misorientation effects and results in a better EMCD signal than the single difference, we divided the data into three categories. For the first two cases, we extracted the EMCD signals by taking the single differences between aperture positions A1, A3 and A4, A2 respectively as used in the conventional 2BC EMCD experiments. In the third case, we extracted the EMCD signal by the double difference of all the four apertures. Figure 5 shows the maximum EMCD signal seen

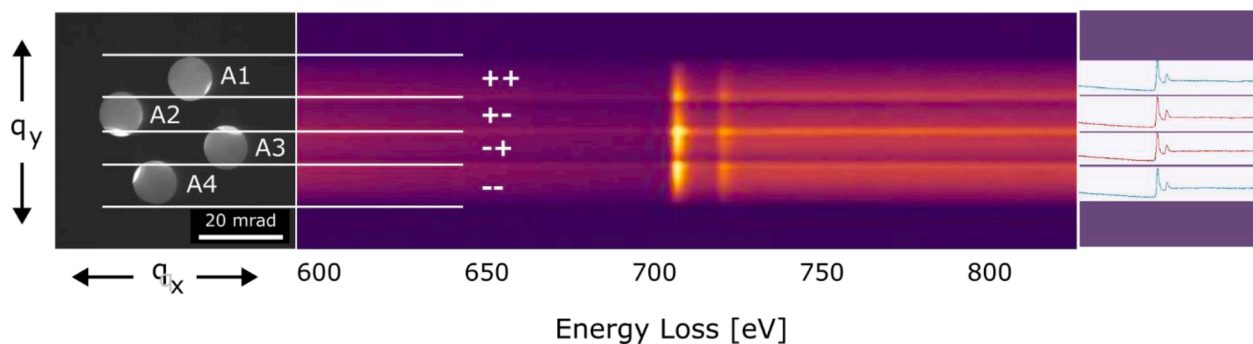


Fig. 3. Left: CCD image of quadruple aperture overlaid on the diffraction pattern, middle: 2D EELS image obtained by integrating the data of all the pixels in the STEM-EMCD map, such an image was acquired at each position while scanning the probe on the sample, right: momentum-resolved raw EELS spectra extracted from the 2D EELS image. These spectra are the summation of all the spectra in the STEM map.

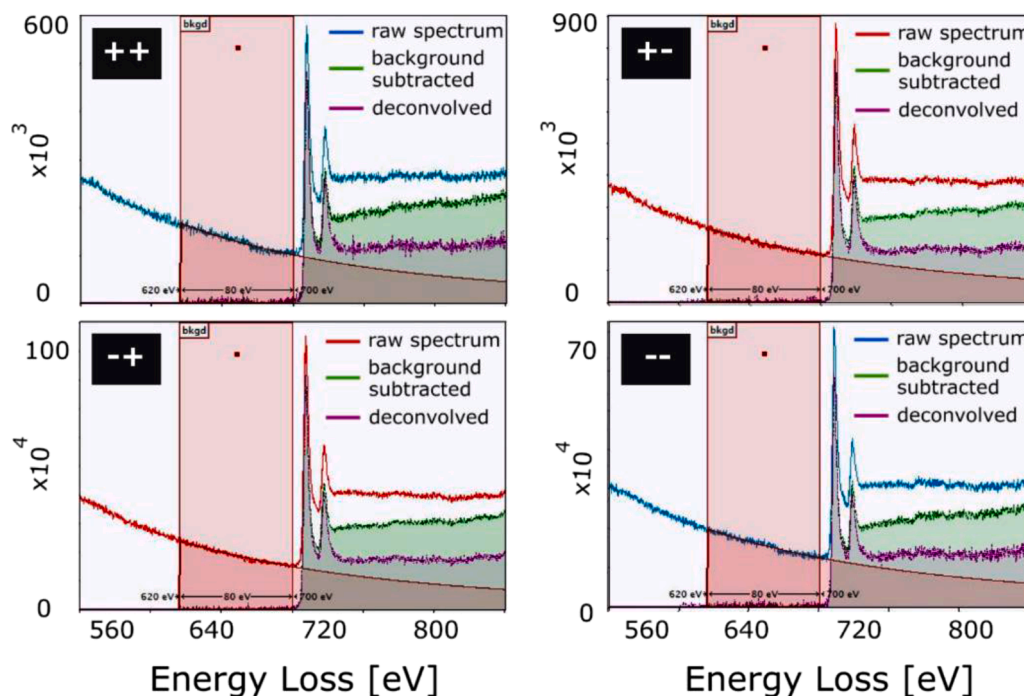


Fig. 4. Raw, background subtracted and deconvolved EELS spectra extracted from the integrated STEM-EMCD map for the four aperture positions. The spectra shown are obtained by summing up all the spectra at each aperture position in the momentum-resolved STEM map.

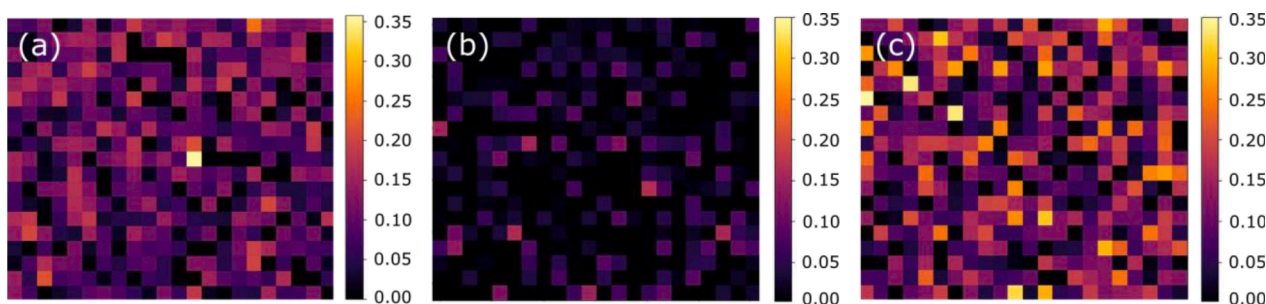


Fig. 5. Maximum EMCD signal seen at Fe- L_3 edge for single differences between (a) A1-A3 (b) A4-A2 and (c) the double difference.

at L_3 edge for each pixel in the map in these three cases. There is a reasonable EMCD signal in case (a) whereas it gets very weak and disappears at most of the pixels for case (b). These significant differences between the two maps are caused by slight changes in underlying diffraction conditions. In this case, the crystal was probably misoriented

from the 3-beam condition in a way that $g=002$ was closer to 2BC, improving the EMCD signal found at aperture positions A1-A3 whereas the EMCD signal at aperture positions A4-A2 went very weak as $\bar{g} = 00\bar{2}$ was far away from 2BC. When doing the STEM-EMCD experiment in a 2-beam condition, there is a decent probability to fall into situation (b) and

end up with a very weak or no EMCD signal. However, the map obtained by double difference (Fig. 5 (c)) shows the best results as not only the EMCD signal is recovered at most of the pixels, but the strength of the signal also goes up compared to the other two maps. This means the double difference eliminates to a great extent, the negative effects induced by orientation changes or asymmetry in agreement with simulations and experiment [18,19].

An important step in the processing of EELS spectra to extract the EMCD signal is to normalize the post-edge intensity of two chiral spectra, under the assumption that the post-edge does not contain magnetic information. For a reliable EMCD signal, the post-edges of the two spectra must be very well aligned after the normalization, as any differences in the post-edge intensities will result in a residual slope in the EMCD signal, complicating the quantification. We applied the standard post-edge normalization to the three cases mentioned above and compared the results in Fig. 6. For normalization, we used a 50 eV window in the interval 750–800 eV. It can be observed that after the normalization, the post-edges do not align very well for the single difference cases (between A1–A3 and A4–A2 apertures) due to slightly different post-edge slopes of the two spectra. These variations in the post-edge intensities of the two spectra can be a result of the slight misalignment of diffraction pattern with respect to the quadruple aperture, contributing uneven intensities at different aperture positions. Another possible source for these intensity variations may be the orientation changes within the scanned region. Nevertheless, we observe that when we use the double difference approach, the post-edges of the two resulting chiral spectra after normalization are very well aligned to each other, even up to an extended energy loss range. This really emphasizes the advantage of double difference procedure for quantitative EMCD.

Finally, we extracted the overall EMCD signal by integrating all the data points in the deconvolved STEM-EMCD map and applying the double difference procedure. The result is shown Fig. 7. The background subtraction and post-edge normalization of the EELS spectra, curve fitting to the resulting EMCD signal and magnetic orbital to spin moments' ratio (m_L/m_S) calculation was done by the procedure and MATLAB code described in ref. [23]. The resulting value of m_L/m_S is 0.07. The m_L/m_S values for bcc Fe reported by previous EMCD experiments [11,12,20,30,36] have differences due to the sensitivity of EMCD experiments on dynamical diffraction conditions. The most accepted value for the ratio is the one reported by XMCD [37] which is 0.04 for bcc Fe. Our resulting value is higher than the value reported by XMCD. There can be several reasons for this over-estimated value. It may be due to the presence of MgO substrate under the magnetic Fe film as previously reported [38]. Contamination built on the specimen during the beam scan may also be a contributing factor. More precisely, the weak EMCD signal strength due to higher thickness of Fe film as well as noise

are the most limiting factors to obtain the best possible quantitative values. In our experience, the noise in the EMCD signal deteriorates the L_2 signal more than the L_3 signal that will cause an overestimation of the ratio where L_2 signal is in the denominator.

4. Discussion

In our previous EMCD work under a 2-beam condition [20], we have shown how strongly the EMCD signal varies as a function of small changes in crystal orientations. The strong differences seen between the EMCD signals at aperture positions A1–A3 and A4–A2 are most probably a result of such slight misorientations in the region scanned by the electron beam. Considering that most of the crystals are not perfect single crystals, such small spatial deviations would be encountered in almost every experiment. The misalignment of post-edge regions due to different slopes is also a contributing factor to the strong variations seen in single difference maps. This post-edge misalignment may be a consequence of orientation changes but is not confirmed at the moment and needs to be explored in more detail. The point to be noted is that taking the double difference in the same data results in a more reliable EMCD signal and a very well aligned post-edge, simplifying the quantification process. So, we reiterate the worth of double difference approach for quantitative EMCD analysis.

The EMCD signal shown in Fig. 7 is obtained by the summation of all the spectra in the STEM map but it is still quite noisy. Apart from the inherently weak signal to noise ratio of the EMCD signal, there are several other reasons for the noise. The convergence semi-angle used for this experiment is relatively large (7.5 mrad) and the EMCD signal strength goes down with increasing convergence angles [27]. Moreover, the experiments were performed on a JEOL 2100 F equipped with a Gatan tridien energy filter. This microscope does not support a nano-beam diffraction mode and the convergence angles resulting in normal STEM mode were too large for the EMCD experiment. To lower the convergence angles, we tuned the mini-condenser lens setting in combination with other lenses. Lowering the beam convergence by increasing the current in mini-condenser lens causes a reduction in probe intensity and induces scan distortions. The scan distortions can be corrected by aligning the beam shift and beam tilt to the optical axis up to a threshold value of mini-condenser lens. The beam current can be increased by tuning the value of C1 condenser lens but it has a reverse effect on convergence angle and makes it larger. Under the compromised conditions obtained during the experiment, we could go down to 7.5 mrad beam convergence angle with a probe current of few picoamps. We compensated for the low probe intensity by using a dwell time of 1 s per pixel for the EMCD acquisition, but a longer dwell time caused higher contamination during the scan. Another experimental challenge on this instrument is the unavailability of magnification reduction function

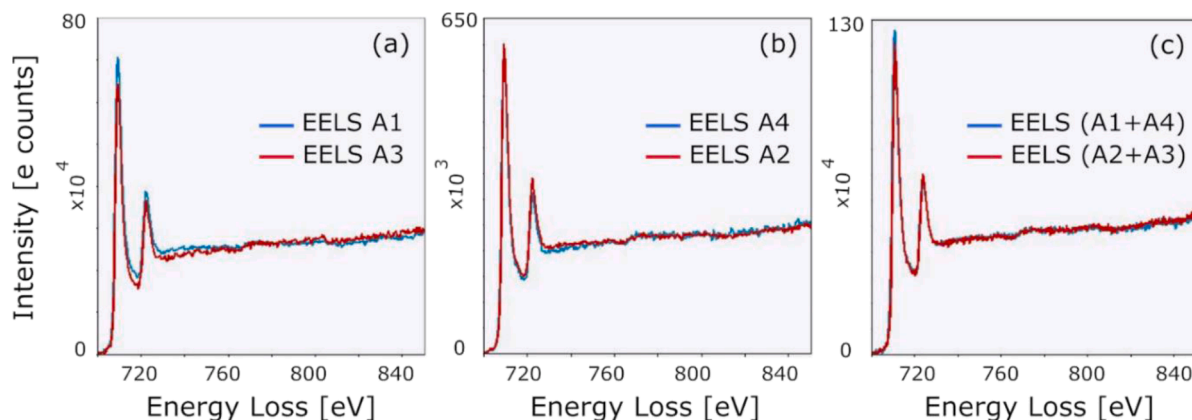


Fig. 6. Post-edge normalized EELS spectra for single differences (a) A1–A3 (b) A4–A2 and (c) the double difference procedure. The spectra shown are obtained by summing up all the spectra in the map.

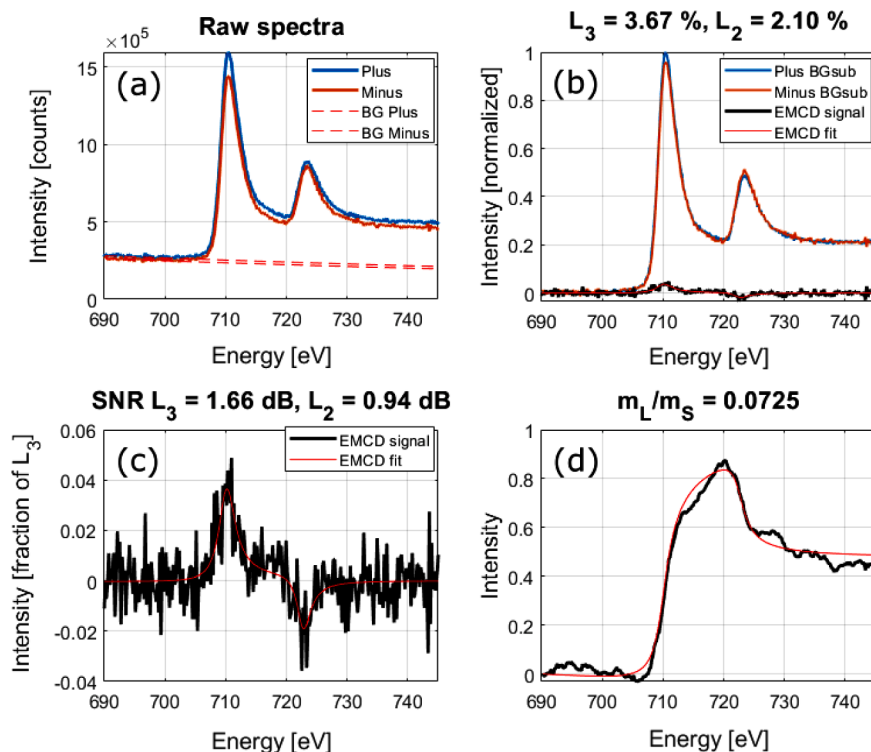


Fig. 7. (a) raw EELS spectra obtained by summing up all the spectra in the STEM map. Here, Plus is the summation of ++ and – signals whereas Minus is the summation of +– and –+ signals (b) Plus and Minus spectra after background subtraction and post-edge normalization, the difference of the spectra is shown as the EMCD signal (c) EMCD signal fitted by a double-Gaussian curve (d) magnetic orbital to spin moments' ratio (m_L/m_S) calculated from the fitted curve.

while using GIF. Even the lowest camera length available in the microscope was too large for the EMCD experiment when projected to the GIF CCD. The camera length was significantly lowered by tuning the currents in intermediate and projector lenses. This step also induces distortions in the diffraction pattern and an optimum setting was found for the values of intermediate lenses (1 and 2) and projector lens. To keep everything according to the optimum settings, we preferred to physically rotate the sample during the experiment instead of further changing the post-specimen lens currents. Finally, we acquired the momentum-resolved EELS data in 4DSTEM format on GIF CCD which is not an optimum detector for such experiments. All these experimental challenges, particularly low probe current and contamination are the key sources for higher noise seen in the final EMCD signal. Despite these experimental challenges, we could still get an EMCD signal strength of nearly 4 % as predicted by the simulations which is an achievement of our single scan setup. Thus, we believe that the same setup if combined with a probe-corrected TEM equipped with a better detector should be able to obtain EMCD signals with considerably higher quality under convergent beam conditions.

Another factor influencing the signal to noise ratio of EMCD signal is the collection angle of each aperture hole. If we consider A as the distance between the center of direct beam to the center of detector (++), the optimum radius for each collection aperture is limited to $r_{opt} = A/3$, under the conditions that the apertures do not overlap to each other as shown in Fig. 8(up). In this experiment, we wanted to verify that the double difference procedure suppresses the asymmetry artefacts and is efficient for a clean EMCD signal extraction, so it was desired to have four individual spectra for this work. Once we establish that the method works well, one could use an alternative 4-hole design where only three individual spectra are extracted from CCD while still realizing the double difference extraction of EMCD signal (Fig. 8(down)). In this geometry, we integrate the +– and –+ signals which have the same chirality. The optimum radius of each aperture allowed by this geometry is $r_{opt} = A/2$ which is 1.5 times more than the maximum radius allowed

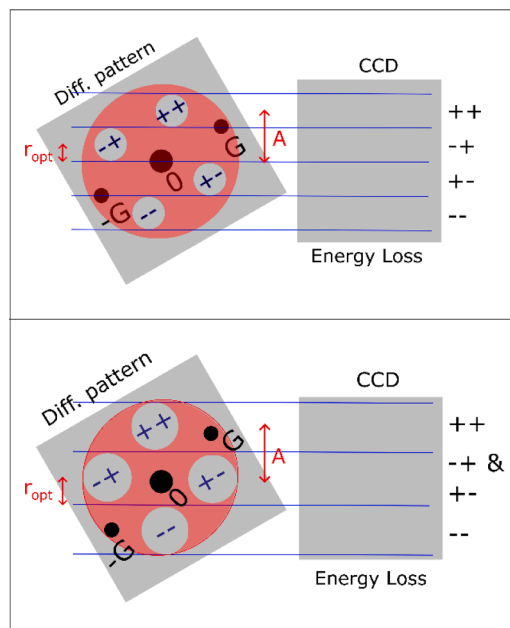


Fig. 8. Up: the quadruple aperture geometry used in this experiment. Down: an alternative aperture geometry allowing larger collection angle of the apertures.

by the geometry used in this experiment. This means an overall improvement of 2.25 times in collection efficiency. Thus, this alternative setup would offer higher signal counts, resulting in an improved signal to noise ratio.

5. Conclusions

We have reported an experimental setup to complete the EMCD experiment is a single STEM scan under 3-beam orientation conditions. With the help of a quadruple aperture, we simultaneously acquire the four momentum-resolved EELS spectra required for the EMCD signal extraction. This can greatly help to remove the EMCD experimental complexities and allow us to precisely correlate the local information contained in the four EELS datasets. We detect a clear EMCD signal for bcc Fe with a beam convergence angle of 7.5 mrad. The setup should be capable to acquire the EMCD signals with higher convergence angles reaching to atomic plane resolution [28].

Declaration of Competing Interest

The authors declare that they have no known competing financial interests or personal relationships that could have appeared to influence the work reported in this paper.

Data availability

Data will be made available on request.

Acknowledgments

H.A, C-W.T and T.T acknowledge the financial support from Swedish Foundation for Strategic Research SSF (ITM17-0301). H.A. gratefully acknowledges Swedish Research Council (project nr. 2021-06748) for their support. T.T acknowledges funding from the Swedish Research Council (project nr. 2016-05113). J.R. acknowledges Swedish Research Council (project no. 2021-03848), Carl Tryggers Foundation and STINT for financial support. The authors are grateful to Toni Uusimäki for developing the GMS script to acquire 4DSTEM data.

References

- [1] P. Schattschneider, S. Rubino, C. Hébert, J. Ruzs, J. Kuneš, P. Novák, E. Carlino, M. Fabrizio, G. Panaccione, G. Rossi, Detection of magnetic circular dichroism using a transmission electron microscope, *Nature* 441 (2006) 486.
- [2] D. Song, Z. Wang, J. Zhu, Magnetic measurement by electron magnetic circular dichroism in the transmission electron microscope, *Ultramicroscopy* 201 (2019) 1.
- [3] Z. Wang, et al., Atomic scale imaging of magnetic circular dichroism by achromatic electron microscopy, *Nat. Mater.* 17 (3) (2018) 221.
- [4] J. Ruzs, S. Muto, J. Spiegelberg, R. Adam, K. Tatsumi, D.E. Bürgler, P.M. Oppeneer, C.M. Schneider, Magnetic measurements with atomic-plane resolution, *Nat. Commun.* 7 (2016) 12672.
- [5] Z.Q. Wang, X.Y. Zhong, R. Yu, Z.Y. Cheng, J. Zhu, Quantitative experimental determination of site-specific magnetic structures by transmitted electrons, *Nat. Commun.* 4 (2013) 1.
- [6] J.C. Idrobo, J. Ruzs, J. Spiegelberg, M.A. McGuire, C.T. Symons, R.R. Vatsavai, C. Antoni, A.R. Lupini, Detecting magnetic ordering with atomic size electron probes, *Adv. Struct. Chem. Imaging* 2 (2016) 1.
- [7] T. Thersleff, S. Muto, M. Werwiński, J. Spiegelberg, Y. Kvashnin, B. Hjörvarsson, O. Eriksson, J. Ruzs, K. Leifer, Towards sub-nanometer real-space observation of spin and orbital magnetism at the Fe/MgO interface, *Sci. Rep.* 7 (2017) 44802.
- [8] R.C. Che, C.Y. Liang, X. He, H.H. Liu, X.F. Duan, Characterization of magnetic domain walls using electron magnetic chiral dichroism, *Sci. Technol. Adv. Mater.* 12 (2011) 25004.
- [9] Z. Li, et al., Atomic structure and electron magnetic circular dichroism of individual rock salt structure antiphase boundaries in spinel ferrites, *Adv. Funct. Mater.* 31 (2021), 2008306.
- [10] K. Xu, T. Lin, Y. Rao, Z. Wang, Q. Yang, H. Zhang, J. Zhu, Direct investigation of the atomic structure and decreased magnetism of antiphase boundaries in garnet, *Nat. Commun.* 13 (2022) 1.
- [11] T. Thersleff, J. Ruzs, S. Rubino, B. Hjörvarsson, Y. Ito, N.J. Zaluzec, K. Leifer, Quantitative analysis of magnetic spin and orbital moments from an oxidized iron (1 1 0) surface using electron magnetic circular dichroism, *Sci. Rep.* 5 (2015) 13012.
- [12] H. Lidbaum, J. Ruzs, A. Liebig, B. Hjörvarsson, P.M. Oppeneer, E. Coronel, O. Eriksson, K. Leifer, Quantitative magnetic information from reciprocal space maps in transmission electron microscopy, *Phys. Rev. Lett.* 102 (2009) 1.
- [13] J. Verbeeck, C. Hébert, S. Rubino, P. Novák, J. Ruzs, F. Houdellier, C. Gatel, P. Schattschneider, Optimal aperture sizes and positions for EMCD experiments, *Ultramicroscopy* 108 (2008) 865.
- [14] S. Schneider, D. Negi, M.J. Stolt, S. Jin, J. Spiegelberg, D. Pohl, B. Rellinghaus, S.T. B. Goennenwein, K. Nielsch, J. Ruzs, Simple method for optimization of classical electron magnetic circular dichroism measurements: the role of structure factor and extinction distances, *Phys. Rev. Mater.* 2 (2018), 113801.
- [15] S. Muto, K. Tatsumi, J. Ruzs, Parameter-free extraction of EMCD from an energy-filtered diffraction datacube using multivariate curve resolution, *Ultramicroscopy* 125 (2013) 89.
- [16] D. Song, G. Li, J. Cai, J. Zhu, A general way for quantitative magnetic measurement by transmitted electrons, *Sci. Rep.* 6 (2016) 18489.
- [17] K. Tatsumi, S. Muto, J. Ruzs, T. Kudo, S. Arai, Signal enhancement of electron magnetic circular dichroism by ultra-high-voltage TEM, toward quantitative nano-magnetism measurements, *Microscopy* 63 (2014) 243.
- [18] H. Lidbaum, J.N. Ruzs, S. Rubino, A. Liebig, B.H. Orvarsson, P.M. Oppeneer, O. Eriksson, K. Leifer, Reciprocal and real space maps for EMCD experiments, *Ultramicroscopy* 110 (2010) 1380.
- [19] J. Ruzs, Role of symmetry in quantitative EMCD experiments, <https://Arxiv.Org/Abs/0910.3849> (2009).
- [20] H. Ali, J. Ruzs, T. Warnatz, B. Hjörvarsson, K. Leifer, Simultaneous mapping of EMCD signals and crystal orientations in a transmission electron microscope, *Sci. Rep.* 11 (2021) 2180.
- [21] D. Negi, J. Spiegelberg, S. Muto, T. Thersleff, M. Ohtsuka, L. Schönström, K. Tatsumi, J. Ruzs, Proposal for measuring magnetism with patterned apertures in a transmission electron microscope, *Phys. Rev. Lett.* 122 (2019).
- [22] D. Song, J. Ruzs, J. Cai, J. Zhu, Detection of electron magnetic circular dichroism signals under zone axial diffraction geometry, *Ultramicroscopy* 169 (2016) 44.
- [23] T. Thersleff, L. Schönström, C.-W. Tai, R. Adam, D.E. Bürgler, C.M. Schneider, S. Muto, J. Ruzs, Single-pass STEM-EMCD on a zone axis using a patterned aperture: progress in experimental and data treatment methods, *Sci. Rep.* 9 (2019) 18170.
- [24] H. Ali, D. Negi, T. Warnatz, B. Hjörvarsson, J. Ruzs, K. Leifer, Atomic resolution energy-loss magnetic chiral dichroism measurements enabled by patterned apertures, *Phys. Rev. Res.* 2 (2020), 023330.
- [25] T. Funk, A. Deb, S.J. George, H. Wang, S.P. Cramer, X-ray magnetic circular dichroism—a high energy probe of magnetic properties, *Coord. Chem. Rev.* 249 (2005) 3.
- [26] P. Schattschneider, M. Stöger-Pollach, S. Rubino, M. Sperl, C. Hurm, J. Zweck, J. Ruzs, Detection of magnetic circular dichroism on the two-nanometer scale, *Phys. Rev. B Condens Matter Mater. Phys.* 78 (2008), 104413.
- [27] T. Thersleff, J. Ruzs, B. Hjörvarsson, K. Leifer, Detection of magnetic circular dichroism with subnanometer convergent electron beams, *Phys. Rev. B* 94 (2016), 134430.
- [28] J. Ruzs, J. Spiegelberg, S. Muto, T. Thersleff, M. Ohtsuka, K. Leifer, P.M. Oppeneer, Localization of magnetic circular dichroism spectra in transmission electron microscopy experiments with atomic plane resolution, *Phys. Rev. B* 95 (2017) 1.
- [29] J. Salafraña, J. Gazquez, N. Nicolás Pérezpérez, A. Labarta, S.T. Pantelides, S. J. Pennycook, X. Batlle, M. Varela, Surface functional organic molecules restore magnetism in metal-oxide nanoparticle surfaces, *Nano Lett.* 12 (2012) 54.
- [30] H. Ali, T. Warnatz, L. Xie, B. Hjörvarsson, K. Leifer, Quantitative EMCD by use of a double aperture for simultaneous acquisition of EELS, *Ultramicroscopy* 196 (2019) 192.
- [31] P. Schattschneider, C. Hébert, S. Rubino, M. Stöger-Pollach, J. Ruzs, P. Novák, Magnetic circular dichroism in eels: towards 10 nm resolution, *Ultramicroscopy* 108 (2008) 433.
- [32] J. Ruzs, Modified automatic term selection v2: a faster algorithm to calculate inelastic scattering cross-sections, *Ultramicroscopy* 177 (2017) 20.
- [33] T. Malis, S.C. Cheng, R.F. Egerton, EELS log-ratio technique for specimen-thickness measurement in the TEM, *J. Electron. Microsc. Tech.* 8 (1988) 193.
- [34] J. Ruzs, S. Rubino, P. Schattschneider, First-principles theory of chiral dichroism in electron microscopy applied to 3D ferromagnets, *Phys. Rev. B* 75 (2007), 214425.
- [35] R.F. Egerton, *Electron Energy-Loss Spectroscopy in the Electron Microscope*, Springer US, Boston, MA, 1996.
- [36] B. Warot-Fonrose, C. Gatel, L. Calmels, V. Serin, P. Schattschneider, Effect of spatial and energy distortions on energy-loss magnetic chiral dichroism measurements: application to an iron thin film, *Ultramicroscopy* 110 (2010) 1033.
- [37] C.T. Chen, Y.U. Idzerda, H.-J. Lin, N. v Smith, G. Meigs, E. Chaban, G.H. Ho, E. Pellegrin, F. Sette, Experimental confirmation of the X-ray magnetic circular dichroism sum rules for iron and cobalt, *Phys. Rev. Lett.* 75 (1995) 152.
- [38] X. Fu, K. Wu, V. Serin, B. Warot-Fonrose, Q. He, R. Yang, L. Zhang, X. Huang, Electron energy-loss magnetic chiral dichroism of magnetic iron film affected by an underlayer in a double-layer structure, *Appl. Phys. Lett.* 115 (2019), 112401.